Applied Energy 352 (2023) 121881

Contents lists available at ScienceDirect

Applied Energy

journal homepage: www.elsevier.com/locate/apenergy

A reconfiguration method for photovoltaic array of stratospheric airship based on multilevel optimization algorithm

Chuan Shan [a], Kangwen Sun [a,b,*], Xinzhe Ji [a], Dongji Cheng [a]

[a] School of Aeronautic Science and Engineering, Beihang University, 37 Xueyuan Road, Beijing 100191, PR China
[b] Yunnan Innovation Institute, Beihang University, 8 Shibo Road, Kunming 650233, PR China

HIGHLIGHTS

- Mismatch loss of stratospheric airships PV array has been raised.
- A multilevel reconfiguration optimization algorithm for PV array have been designed.
- The output characteristics of PV array before and after reconfiguration are compared.
- The necessity of the PV reconfiguration system on the airship is proven.

ARTICLE INFO

Keywords:
Photovoltaic array
Stratospheric airship
Reconfiguration
Optimization algorithm
Mismatch loss
Energy improvement

ABSTRACT

Reducing the mismatch loss to increase the output power of the photovoltaic (PV) array is crucial for extending the flight time of stratospheric airships. This paper presents a reconfiguration system for PV arrays based on a switch matrix designed for stratospheric airships. The proposed system employs a multilevel optimization reconfiguration algorithm that combines smart choice, greedy, and Munkres' assignment algorithms. Simulations were conducted under single working conditions, full-day sunlight cycles, and full-year PV array reconfigurations, respectively. The results demonstrated that the reconfigured PV array significantly improved the output power with a smooth P—V curve. The instantaneous power under extreme working conditions could be increased by 50.1%. Furthermore, during the 7-day simulation process, the average daily power output of the PV array increased by 14.68%, whereas the output fluctuation during circular cruising was reduced. The reconfiguration system offers greater advantages during months with weak irradiance in high-latitude regions, where the daily output power of the PV array can be increased by up to 24.46%. This significantly reduces the installation area and weight ratio of a stratospheric airship PV array.

1. Introduction

Compared to solar-powered aircraft and high-altitude balloons, stratospheric airships have the advantages of maneuverability, controllability, the ability to maintain high altitudes for a long time [1], and the ability to carry heavy loads [2], which makes them better suited for tasks such as regional surveillance, ground monitoring, and communication relays [3,4]. A stratospheric airship utilize a photovoltaic (PV) array [5,6], energy storage system, and energy management system [7,8] to provide continuous power to its avionic and propulsion systems, thereby enabling long-duration flights [9,10]. Enhancing the power capacity and reliability of the cyclic energy system is a pivotal aspect in prolonging the airship's endurance. Research in this area has focused on the three aspects described below.

First, optimization of the arrangement of solar cells, which is an effective method for enhancing the energy production capacity of PV arrays. Wang et al. [11] initially proposed a numerical computational method for assessing the solar radiation distribution on the PV array of a stratospheric airship. Li et al. [12,13] introduced a solar cell thermal model to refine the aforementioned method and applied a genetic algorithm to optimize the layout of a PV array, resulting in a maximum improvement of 25% in its power output capacity in specific scenarios. Alam [14] proposed a multidisciplinary optimization method for stratospheric airship based on a genetic algorithm that obtained the optimal layout for a solar array with five deployment locations.

Second, joint optimization of the wind field, flight trajectory, and

* Corresponding author at: School of Aeronautic Science and Engineering, Beihang University, 37 Xueyuan Road, Beijing 100191, PR China.
E-mail address: sunkw100@buaa.edu.cn (K. Sun).

https://doi.org/10.1016/j.apenergy.2023.121881
Received 30 April 2023; Received in revised form 29 July 2023; Accepted 2 September 2023
Available online 18 September 2023

flight attitude, as an effective approach for enhancing the energy acquisition of PV arrays. Zhu et al. [15]proposed a method to enhance the output capacity of PV arrays in the quasi-zero wind layer by optimizing the yaw angle. The simulation results demonstrated the advantages of this optimization approach, particularly in the winter seasons in high-latitude regions. Zhang et al. [4] proposed an attitude angle planning strategy that integrates roll, yaw, and pitch controls to enhance the energy production of PV arrays and the wind resistance of airships. Shan et al. [16] proposed a flight strategy for stratospheric airships based on positional energy storage. This strategy enables the redistribution of energy, thereby enhancing the endurance of airships within the designated mission area.

The third approach involves enhancing the power- supply capacity of the energy system using a PV tracking system [17]. Li et al. [18] designed a PV array irradiance tracking system that can rotate radially around an airship, resulting in a daily energy output increase of more than 40%. Du [19]and Zhu [20] conducted relevant studies on comprehensive optimization strategies for thermal characteristics, rotation, and yaw angles in real wind fields for this system. Owing to the considerable challenges in structural design and center-of-gravity control, the application of this system to stratospheric airships has not yet been realized.

Various methods have been proposed for enhancing the power output of PV arrays in stratospheric airships. However, the effect of the interconnection method of curved PV arrays on their performance has not yet been investigated. Liu et al. [21] proposed an energy-efficiency evaluation method for PV arrays under shaded conditions and studied the output capabilities of four connection configurations: series–parallel (SP), bridge-link (BL), honeycomb (HC), and, total cross-tied (TCT) connections. The results indicate that the performance of the TCT connection surpasses those of the SP, BL, and HC. Despite the improved performance of the TCT connection, the mismatch losses in the case of local shading conditions still lead to significant performance degradation, severely reducing the output capacity of the curved PV arrays.

Dynamic reconfiguration technology is regarded as an effective method for mitigating the overall impact of local shading on ground-mounted PV systems. Valasco-Quesada et al. [22] initially proposed the equalization index (EI) as an optimization metric for evaluating TCT configurations. Candela et al. [23] and Romano et al. [24] introduced a fully reconfigurable dynamic electrical scheme (DES) for PV generators and compared the performance of two reconfiguration algorithms: random search and deterministic. Riva et al. [25] proposed a straightforward dynamic programming algorithm to modify the switch layout to maximize the output of PV modules under shading conditions. Jazazyeri et al. [26] generated irradiance profiles using real-sky images and multiple cloud types and proposed a PV array reconfiguration algorithm that seeks to find near-optimal array configurations. The multisource and stochastic nature of shading in ground PV systems increases the difficulty of prediction and assessment. Therefore, various adaptive algorithms have been developed to enhance the accuracy and real-time performance of optimal configurations , including scanning algorithms [27], feed-forward neural networks [28], fuzzy controls [29], and heuristic algorithms [30–32]. Other switch connections have also been proposed to enhance the output power of the PV arrays. Nguyen et al. [33] divided the PV array into fixed and adaptive parts. Compensation for shadows in the fixed part through modules in the adaptive part mitigates this mismatch. Chao et al. [34] designed novel connections that involved installing connecting switches between branches. This approach allows for the control of modules in shadow or fault modes through switches, thereby increasing the power output of the system. Cynthia et al. [35] proposed dividing the array into equal quantities of female and male parts to enhance the output power of the array by optimally matching the rows in both parts. Ramasamy et al. [36] proposed a novel reconfigured connection scheme. Compared with TCT connections, this connection scheme exhibits significant advantages in shadow management, effectively eliminating multiple peaks in the power curve.

In contrast to ground PV systems, uneven irradiation is a typical characteristic of airship PV arrays. This persists and varies with the airship's attitude angle and flight duration. Approaches and methods to mitigate the detrimental impacts of mismatch losses caused by the nonuniformity of irradiance in TCT-configured airship PV arrays have not been investigated.

The main novelty of this study is the integration of the reconfiguration concept from ground PV systems with stratospheric airship PV arrays to address mismatch issues. By utilizing the dynamic electrical scheme switching matrix (DESSM) and the electrical characteristics of airships, a reconfiguration system for stratospheric airship PV arrays was devised. The concept of a coordinate matrix for airship PV arrays was introduced. An advanced multilevel optimization algorithm incorporating the smart choice algorithm (SCA), greedy algorithm (GA), and Munkres' assignment algorithm (MAA) was designed to mitigate the mismatch loss caused by the non-uniform distribution of radiation. This algorithm aims to efficiently compute a configuration that is close to optimal while minimizing the utilization of computational resources. Moreover, a reduction in nonessential switching operations is considered to prolong the lifespan of the switching matrix. Airship residence in real wind fields and real-time PV array reconfigurations were simulated. The results illustrate that the reconfigured system significantly enhanced the energy output of the PV array and mitigated the output power fluctuations caused by changes in attitude angles. Furthermore, the improvement rates of the reconfiguration of the airship PV array energy output across different latitudes and months were analyzed. This study can effectively enhance the output performance of the airship PV array while significantly reducing the installation area and weight ratio of the PV array.

2. Solar radiation model of curved PV array

2.1. Solar radiation model

Firstly, it is necessary to establish a mathematical model that describes the regularity of the sun's movement. As the distance between the sun and the earth changes over time, and the plane of the earth's rotation is at a certain angle to the plane of the ecliptic, an eccentricity correction factor e_r needs to be introduced:

As shown in Fig. 1, the basic parameters for describing the position of the sun are the day angle θ_{day}, declination angle θ_{dec}, altitude angle θ_{ele}, azimuth angle θ_{azi}, and hour angle θ_{hour}. The formulas for calculating each parameter are as follows [37,38]

$$\begin{aligned}
&\theta_{azi} = arccos\left(\frac{sin(\theta_{ele})sin(\Phi) - sin(\theta_{dec})}{cos(\theta_{ele})cos(\Phi)}\right)\\
&\theta_{dec} = 0.3723 + 23.2567\cdot sin(\theta_{day}) + 0.1149\cdot sin(2\cdot\theta_{day}) - 0.1712\cdot sin(3\cdot\theta_{day})\\
&\qquad -0.758\cdot cos(\theta_{day}) + 0.3656\cdot cos(2\cdot\theta_{day}) + 0.0201\cdot cos(3\cdot\theta_{day})\\
&\theta_{ele} = arcsin(sin(\theta_{dec})sin(\Phi) + cos(\theta_{dec})cos(\Phi)cos(\theta_{hour}))\\
&\theta_{day} = \frac{(d_n - N_r)}{365.2422}\\
&\theta_{hour} = (time + e_t/60 - 12)\cdot 15
\end{aligned} \tag{1}$$

where Φ represents the local latitude, *time* represents the local time, d_n is the day number in a year, N_r is the correction term of the day number.

To calculate the radiation intensity of the sun reaching the stratospheric airship flying at altitude, the atmospheric transparency τ_h and air quality ratio *amr* are first given by [39,40]

$$\begin{aligned}
&\tau_h = 0.5\cdot\left(e^{-0.65\cdot amr} + e^{-0.095 amr}\right)\\
&amr = \left(\frac{p_h}{p_0}\right)\cdot\left[\sqrt{1229 + (614\cdot sin(\theta_{ele}))^2} - 614\cdot sin(\theta_{ele})\right]
\end{aligned} \tag{2}$$

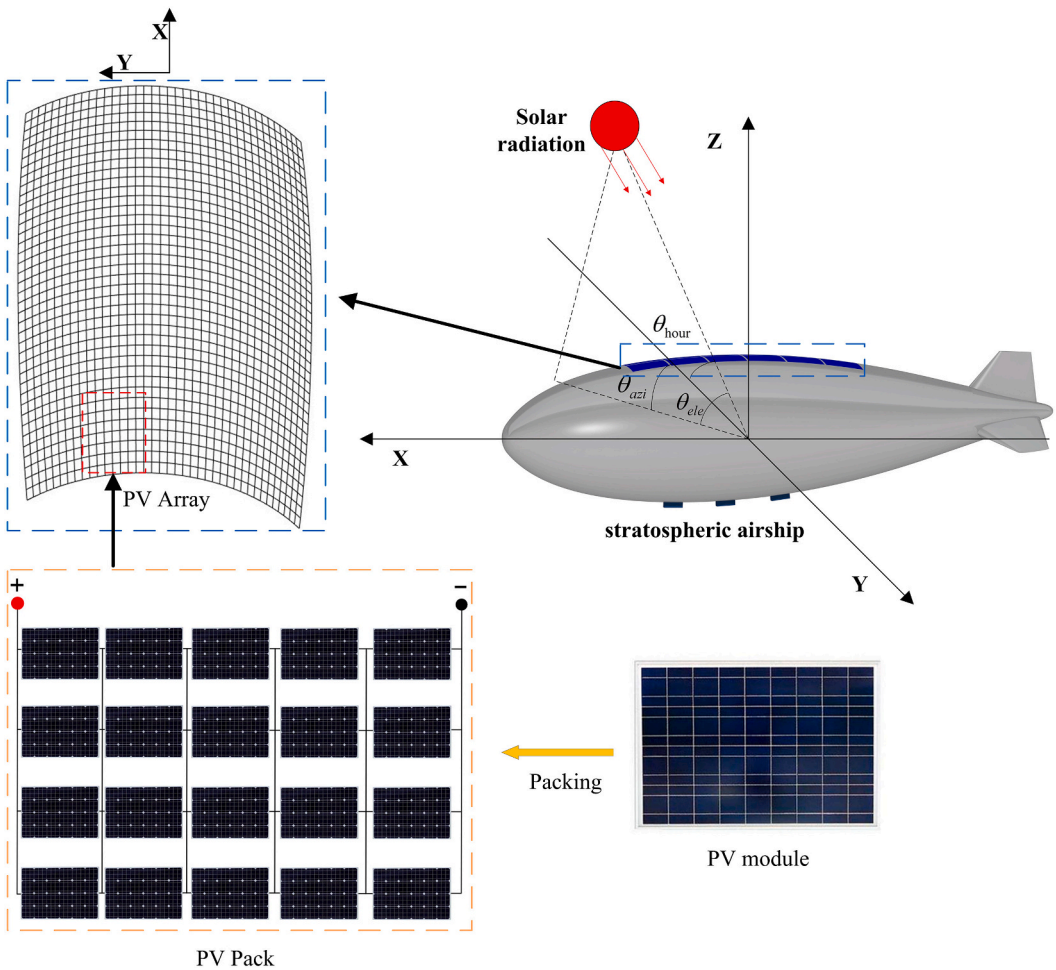

Fig. 1. Composition of the photovoltaic (PV) array on stratospheric airship.

where p_h is the air pressure at the altitude of the airship, and p_0 is the sea level air pressure.

The direct radiation intensity I_{h0} reaching the altitude of the stratospheric airship can be calculated as [41]

$$I_{h0} = \tau_h \cdot \left(\frac{1 + e_e \cdot cos(\lambda_e)}{1 - e_e^2} \right) \cdot 1367 \tag{3}$$

where e_e is the eccentricity of the Earth taken as 0.016708, and λ_e is the eccentricity correction coefficient, given by [42]

$$\lambda_e = \theta_{day} + 2e_e \cdot sin(\theta_{day}) + 1.25e_e^2 \cdot sin(2\theta_{day}) \tag{4}$$

The scattering of sunlight at the altitude of the stratospheric airship I_{dh} is calculated as

$$I_{dh} = 0.5 \cdot sin(\theta_{ele}) \cdot \frac{amr(1 - \tau_h)}{amr - 1.41 \cdot \tau_h} \cdot \left(\frac{1 + e_e \cdot cos(\lambda_e)}{1 - e_e^2} \right) \cdot 1367 \tag{5}$$

2.2. Curved PV array model

Generally, the shape of an airship can be considered as a rotational solid obtained by rotating a planar curve around a symmetry axis. Based on the theory of rotational bodies, a finite element model of the surface curvature array for the airship is established. The equation for the control surface of its surface is defined as

$$F = x^2 + y^2 - z^2 \tag{6}$$

where z is the rotational radius of the airship, which is a function of x. x and y are the axial and radial coordinates of the airship, respectively, as shown in Fig. 1. In this study, the GNVR−50 configuration of the airship is selected, and z is expressed as follows

$$\begin{cases} z = \sqrt{0.25D^2 \cdot \left(1 - \frac{(x - 1.25D)^2}{1.5625D^2}\right)} & 0 \le x < 1.25D \\ z = \sqrt{16D^2 - (x - 1.25D)^2} - 3.5D^2 & 1.25D \le x < 2.875D \\ z = \sqrt{0.1373D \cdot (1.7998D - (x - 1.25D))} & 2.875D \le x < 3.05D \end{cases} \tag{7}$$

where D represents the maximum diameter of the airship. The normal vector of a certain element on the surface of a solar panel can be expressed as

$$n_i = \left(\frac{\partial F}{\partial x_i}, \frac{\partial F}{\partial y_i}, \frac{\partial F}{\partial z_i} \right) \Big/ \sqrt{\left(\frac{\partial F}{\partial x_i}\right)^2 + \left(\frac{\partial F}{\partial y_i}\right)^2 + \left(\frac{\partial F}{\partial z_i}\right)^2} \tag{8}$$

Matrix R represents the transformation matrix from the airship's body coordinate system to the inertial coordinate system. The Euler angles $\eta = [\psi, \varphi, \phi]$ represent the yaw angle, pitch angle, and roll angle of the airship. The transformation matrix can R be given by

$$\begin{bmatrix} C_\varphi \cdot C_\psi & S_\phi \cdot S_\varphi \cdot C_\psi - C_\phi \cdot S_\psi & C_\phi \cdot S_\varphi \cdot C_\psi \\ C_\varphi \cdot S_\psi & C_\phi \cdot C_\psi + S_\phi \cdot S_\varphi \cdot S_\psi & S_\psi \cdot S_\varphi \cdot C_\phi - S_\phi \cdot C_\psi \\ -S_\varphi & C_\psi \cdot S_\phi & C_\phi \cdot C_\varphi \end{bmatrix} \tag{8}$$

The projection coefficient of solar radiation on the surface of the

airship ω_{sign} is calculated by

$$\omega_{sign} = \begin{cases} |n_s \cdot n_{ig}| & n_s \cdot n_{ig} < 0 \\ 0 & n_s \cdot n_{ig} \geq 0 \end{cases} \tag{9}$$

where n_s represents the unit vector of solar radiation in the inertial coordinate system, and $n_{ig}$is the unit normal vector of the element i in the inertial coordinate system. Both are given by

$$\begin{aligned} n_s &= (-cos\theta_{ele} \cdot cos\theta_{azi}, -cos\theta_{ele} \cdot sin\theta_{azi}, sin\theta_{ele}) \\ n_{ig} &= R \cdot n_i \end{aligned} \tag{10}$$

The direct radiation intensity I_{d0i} and scattered radiation intensity I_{dhi} received by the element i of the solar panel can be respectively expressed as

$$\begin{aligned} I_{d0i} &= \omega_{sign1} \cdot I_{d0} \\ I_{dhi} &= 0.5 \cdot (1 - cos(\alpha_i)) \cdot I_{dh} \end{aligned} \tag{11}$$

where α_i represents the angle between the element and the horizontal plane, which is calculated as

$$\alpha_i = arccos\left(\frac{n_{ig} \cdot n_z}{|n_{ig}| \cdot |n_z|}\right) \tag{12}$$

Therefore, the total radiation intensity I_{di} received by the elements of the solar panel is expressed as

$$I_{di} = I_{d0i} + I_{dhi} \tag{13}$$

3. Design of the reconfiguration device for the photovoltaic array

3.1. Connection methods of the photovoltaic array

The PV array on an airship is composed of individual PV modules, which are connected in series to increase the total bus voltage to match the input voltage requirement of the DC–DC converter and connected in parallel to increase the bus current to match the energy demand of the airship during day and night flights. During the operation of a PV array, mismatch loss is one of the main factors affecting the output power. As shown in Fig. 2, many interconnection topology models of arrays have been proposed to reduce mismatch losses, including series, parallel, SP, TCT, BL, and HC connections [43]. Although various interconnection topologies have been developed, SP and TCT connections remain the most widely used and mature connection methods. Unlike ground-based PV systems that are easy to detect and maintain [44], a high level of reliability is required for the interconnection topology of a PV array in an airship to mitigate the impact of individual component failures on the system; thus, the TCT configuration is more suitable for use in airship PV systems. Therefore, this study focuses on the TCT connection as the basic topology of a PV array on a stratospheric airship to conduct system reconfiguration research.

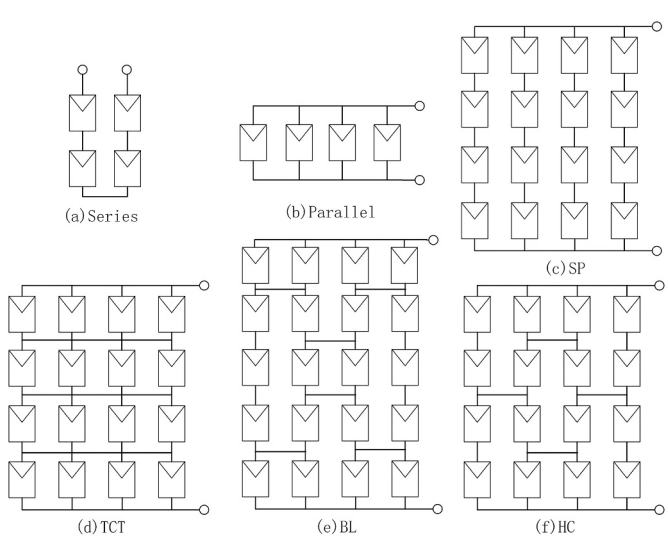

Fig. 2. Typical interconnection structures of PV array.

3.2. Design of switching matrix

Romano et al. [24] introduced a DESSM, as illustrated in Fig. 3. This system employs a switch array and a control module to achieve arbitrary connections of PV modules, including two extreme cases of parallel or series connections of all modules. For a PV array comprising n modules, the DESSM system requires n^2 double-pole switches (DPST) to implement the configuration calculated using the optimization algorithm. Moreover, each row of the DESSM system is equipped with a single-pole switch (SPDT) called a "row switch," which allows for continued current flow when there are no modules in the corresponding row by closing the switch. The total number of switches N_{SW} required for n modules can be calculated as

$$N_{SW} = (n^2)_{DPST} + (n)_{SPDT} \tag{14}$$

To match the working voltage of the propulsion motor and energy storage batteries, as well as to reduce the additional weight of power cables, the PV array of stratospheric airships adopts a "high voltage to sub-high voltage" voltage system. The number of modules in series is determined during the design phase and cannot be changed arbitrarily. Row switches are not necessary, and the number of column switches for each component is determined based on the designed number of series connections of the array. Therefore, the DESSM system can be optimized, as shown in Fig. 4, resulting in a significant reduction in the total number of switches, system complexity, and additional weight. For example, for a 3 × 3 TCT configuration PV array, the total number of switches decreases from 90 to 27. For an m*n PV array, the total number

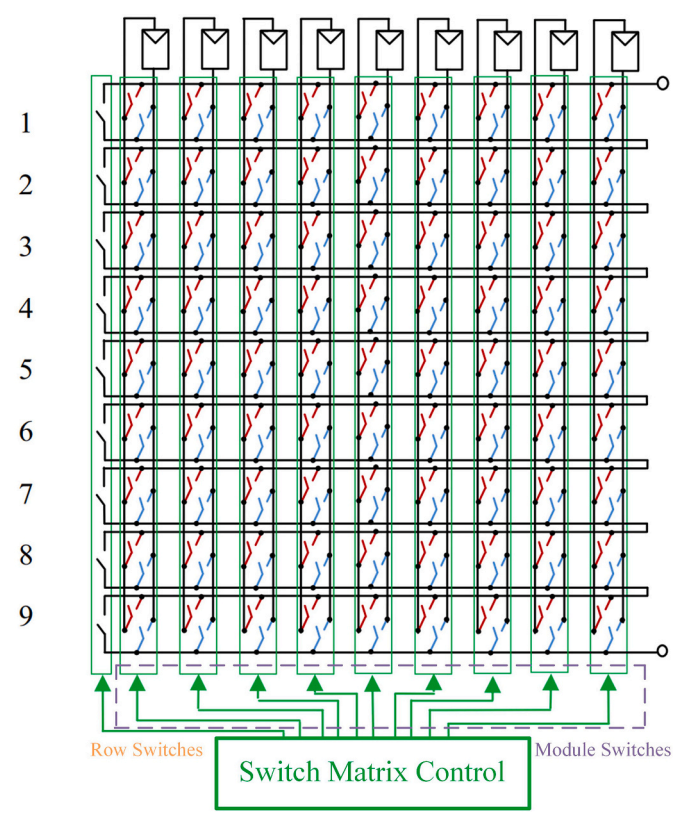

Fig. 3. Dynamic electrical scheme switching matrix (DESSM) [24].

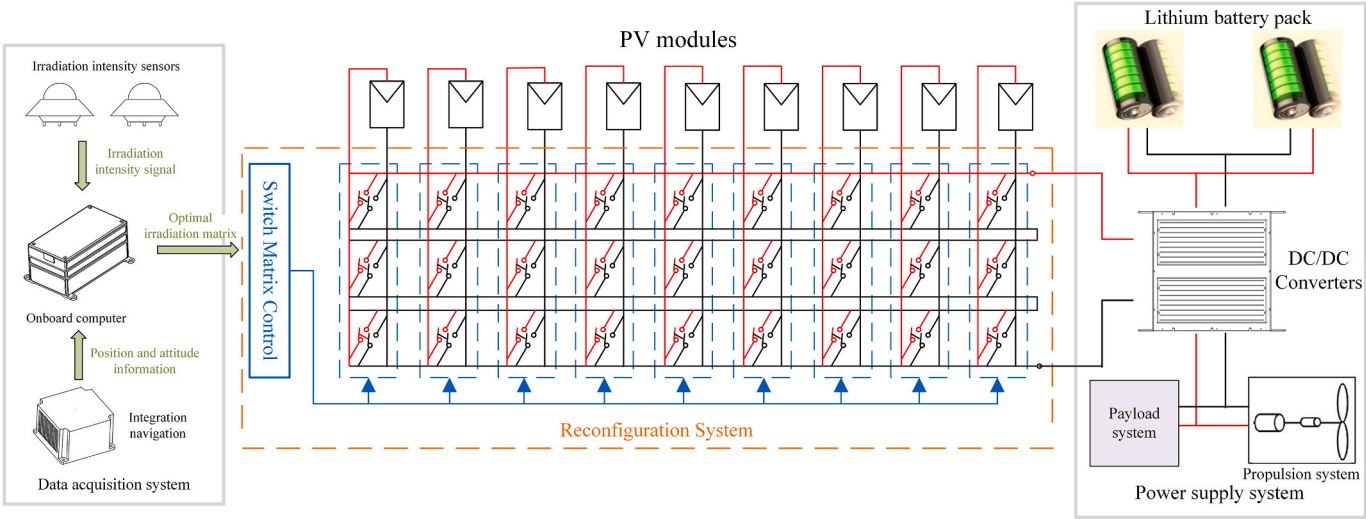

Fig. 4. Stratospheric airship DESSM system.

of switches required for the switch matrix can be simplified as

$$N_{SW} = \left(m^2 \cdot n\right)_{DPST} \tag{15}$$

Moreover, Fig. 4 illustrates the specific implementation of the PV reconfiguration system. The reconfigurable energy system primarily consists of a data acquisition system, a PV reconfiguration system, and an energy supply system. The reconfiguration system and irradiation sensors are situated on the airship's surface, adjacent to the PV array, while the remaining devices are situated within the airship gondola. The on-board computer calculates the optimal irradiation matrix by acquiring the airship's position, attitude, and irradiation intensity. The optimized irradiation matrix is transmitted instantaneously to the switch matrix controller, which then converts it into control signals for the switch matrix to reconfigure PV modules in real-time.

3.3. Photovoltaic array reconfiguration criteria

Manna et al. [45] summarized the electrical characteristics of TCT-configured PV arrays as follows.

(1) The maximum power point (MPP) voltage of each PV module is less affected by the irradiance level.
(2) The current flowing through the PV modules connected in parallel is almost proportional to the irradiance level of each module.

Velasco-Quesada et al. [22] pointed out that, to maximize the available power at the PV array output, it is desirable that none of the series-connected rows of parallel-connected PV modules limit the current flowing in a single string. If the total irradiance and current in each row are comparable, the PV array would achieve maximum output power, which is referred to as the "irradiance equalization" criterion of TCT configuration [46]. The primary objective of reconfiguring the PV array is to achieve power balance in every row by adjusting the positions of the PV modules, thereby avoiding mismatch loss [47].

To calculate the total irradiance of each row for a TCT configuration with m rows and n columns, the irradiance of the PV modules located in rows i and j is defined as I_{ij}. The total irradiance of row i and the mean irradiance of each row are given by

$$\begin{aligned} I_{rowi} &= \sum_{j=1}^{n_i} I_{ij} \\ I_{rowavg} &= \sum_{i=1}^{m} I_{rowi} \Big/ m \end{aligned} \tag{16}$$

For each configuration, the equalization index (EI) is calculated by means of the following expression:

$$EI = max(I_{rowi}) - min(I_{rowi}) \quad \forall i \tag{17}$$

This index quantifies the level of current limitation of the configuration. Therefore, EI is defined as the decision variable of irradiance equalization optimization problem. According to the "irradiance equalization" criterion, the objective function of the reconfiguration optimization algorithm is to minimize the EI, as follows:

$$J = min(EI) \tag{18}$$

In the case of multiple configurations with the same EI, configurations attainable with the minimum number of switching operations will be selected. Section 3.2 mentioned that the number of modules in series is not allowed to change. Therefore, the optimization problem subject to the following constraints:

$$N_{rowi} \geq 1 \quad \forall i \tag{19}$$

where N_{rowi} is the number of non-zero elements in the row vector of the irradiation matrix.

The PV array reconfiguration process is shown in Fig. 5. The sum of the irradiance in each row for the initial configuration was 2820, 2360, 2500, and 2040 W/m^2. After reconfiguration by adjusting the position of the PV modules, the irradiance in each row was balanced at 2680 W/m^2. Fig. 6 compares the P—V curves of the PV array before and after the reconfiguration. The significant difference in irradiance among the rows before reconfiguration resulted in a P—V curve that exhibited multiple MPPs, which caused serious misguidance in the MPP tracking (MPPT) algorithms [48]. Moreover, the power at the MPP was low, at only 2483 W. The power at the single MPP of the P—V curve after reconfiguration was 2940 W, representing an 18.4% improvement, which does not lead to misguidance in the MPPT search algorithms.

4. Reconfiguration algorithm design

4.1. Coordinate matrix

The main reason for the uneven irradiance of ground-based PV systems is local shading caused by nearby buildings, plants, and cloud cover. Such shading is highly random, and it is difficult to predict the irradiance status of the individual modules. Therefore, ground-based PV systems generally calculate current irradiance by comparing the actual output current with the theoretical output current in real time. By

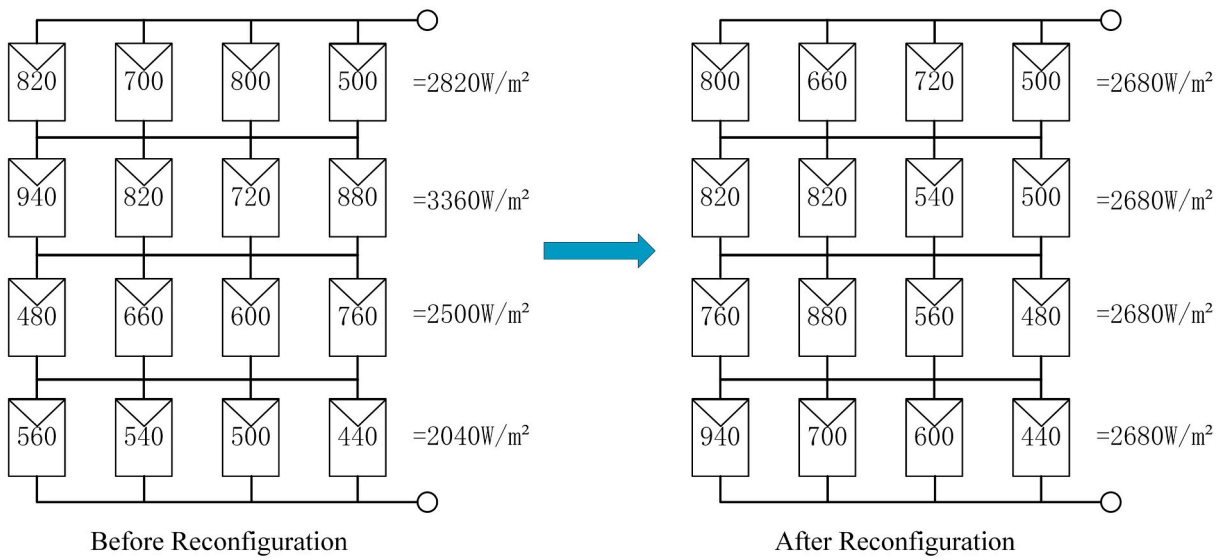

Fig. 5. Schematic of the PV array reconfiguration process.

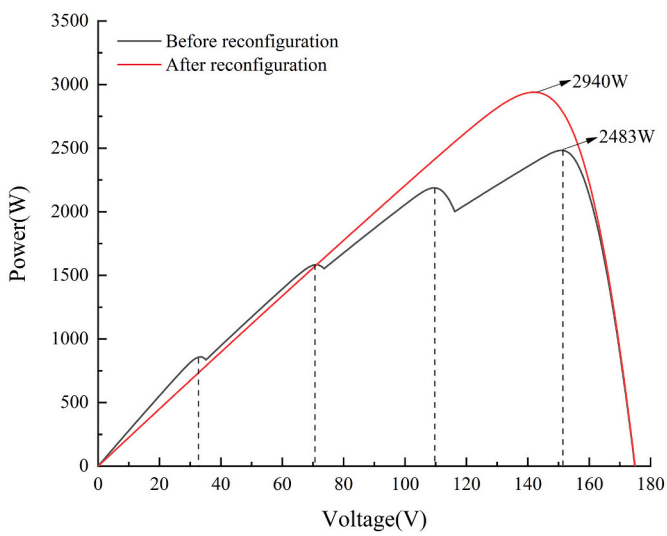

Fig. 6. Comparison of P—V curves before and after reconfiguration.

contrast, at the flight altitude of stratospheric airships, there are no random shading factors, and the irradiance of the PV modules depends solely on their placement on the airship.

Therefore, before designing the reconfiguration algorithm for the PV array of airships, in addition to the "irradiance matrix" that represents the irradiance of the modules, it is necessary to define the "coordinate matrix" that represents the placement position of the modules. Taking the example of a 4 × 4 TCT configuration, with the airship's axial direction defined as a column and the radial direction defined as a row, the irradiance and coordinate matrices can be defined as shown in Fig. 7.

4.2. Smart choice algorithm (SC)

The challenge of achieving irradiance equalization can be considered a subset-sum problem, which can be generalized as follows: Given a set of integers and an integer s, is there any nonempty subset whose sum is equal to s? Sanseverino [25] proposed a dynamic programming (DP) algorithm to address the subset-sum problem. First, the average row irradiance I_{rowavg} for the current configuration is calculated. Subsequently, elements whose irradiance is equal or close are grouped, and each group forms a new row in the matrix.

Ngoc [49] pointed out that the DP algorithm can calculate the optimal solution in most cases; however, in some special matrices, it may not be possible to find the optimal solution because the first row is

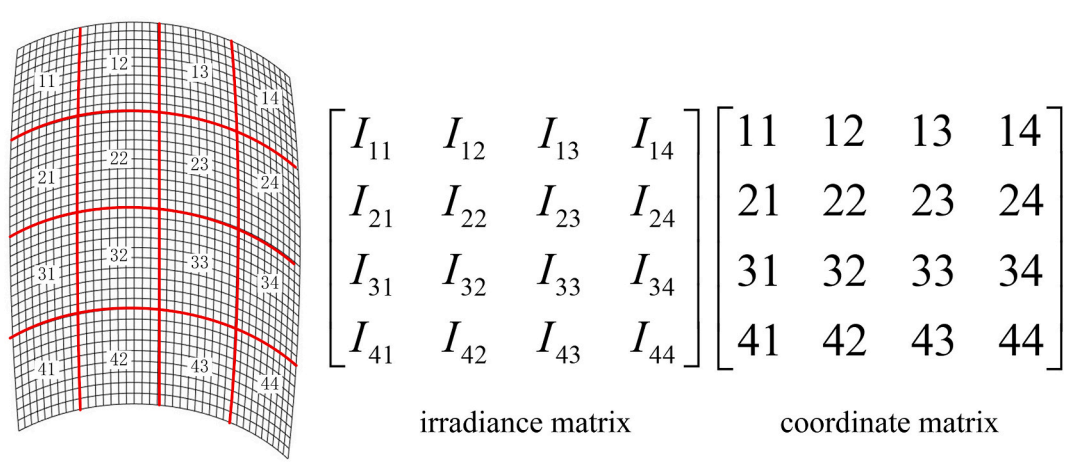

Fig. 7. Schematic of irradiation matrix and coordinate matrix.

filled during the solving process. Furthermore, the DP algorithm typically consists of a series of steps, each with a choice that consumes significant computational resources and requires substantial processing time.

To overcome these issues, Ngoc [49] proposed an intelligent selection algorithm, the smart choice (SC) algorithm, which focuses on global optimization and has a relatively simple calculation process. Owing to the limited computational resources available onboard the airship, the SC algorithm is better suited for the PV array reconfiguration of airships. The calculation steps are as follows:

Step 1: Sort the initial irradiance matrix A in descending order using the quicksort arrangement method to obtain array B and synchronize the corresponding coordinate matrix A_{co} with the sorted array.

Step 2: Original matrix A has m rows. Divide array B into m groups of equal size, and fill the first group's irradiance values and corresponding coordinates in descending order into matrix C and C_{co}.

Step 3: Subsequently, fill each group in descending order. The filling criteria are as follows: the module with the highest current irradiance is filled in the row with the lowest irradiance value from the previous round, the module with the second-highest irradiance value is filled in the row with the second-lowest irradiance value, and so on. The filling process continues in this manner, and the C_{co} matrix is synchronized with the filling of C.

Step 4: Repeat step (3) until all the groups in B have been filled, and a new matrix C is formed.

Taking the initial irradiance matrix shown in Fig. 5 as an example, the optimization process of the SC algorithm is shown in Fig. 8.

4.3. Greedy algorithm (GA)

The SC algorithm quickly reconstructs the original matrix into a new matrix by performing rapid descending sorting and one recombination, resulting in a significant reduction in the EI. Despite its simplicity and speed, the SC algorithm may only yield suboptimal solutions in certain scenarios, and the optimal solution may not necessarily take the form of an n × n matrix, in which the number of parallel modules in each row is not necessarily identical. Hence, it is necessary to devise an algorithm that can achieve a globally optimal solution based on the C matrix obtained from the SC algorithm while simultaneously demanding fewer computations.

Mahmoud [50] proposed a PV array reconfiguration solution method based on a greedy algorithm (GA). The fundamental concept of this algorithm is to decrease the current EI value by shifting or exchanging the PV modules between rows until the EI cannot be further reduced. Although each step of the GA optimizes the current outcome, it cannot further minimize the EI after multiple iterations. The optimal solution at this stage constitutes the global optimal solution.

Mahmoud's GA was intended for partially shaded PV arrays comprising fixed and reconfigurable groups [50]. The asynchronous execution of swapping and moving operations leads to an increase in the number of computational steps. Following the pre-optimization of the irradiance matrix using the SC algorithm, the GA can perform simultaneous swapping and moving operations, facilitating the identification of a more optimal solution. Therefore, this study proposes the following improvements to the process.

Step 1: Calculate the cumulative sum of the irradiance for each row of the preoptimized matrix C obtained using the SC algorithm.

Step 2: The rows with the highest and lowest irradiance values in matrix C can be adjusted in two ways.

(a) Swapping an element between two rows.

(b) Transferring an element from the row with the maximum irradiance to the row with the minimum irradiance.

Step 3: Enumerate all the schemes in step (2) and select the adjustment scheme with the lowest EI for each.

Step 4: Compare adjustment schemes (a) and (b), and select the one with the lowest EI.

Step 5: Validate the effectiveness of the GA. Adjustment proposals are accepted only if the EI obtained in step (4) is lower than the initial EI.

Step 6: The aforementioned steps are repeated until balance no longer improves. The detailed process is as follows:

(a) If the adjustment is approved in step 5, update C and C_{co} matrices.

(b) Otherwise, steps 2–5) are repeated between the row with the lowest irradiance value and the second-highest row (and subsequently the third-highest, fourth-highest, etc.).

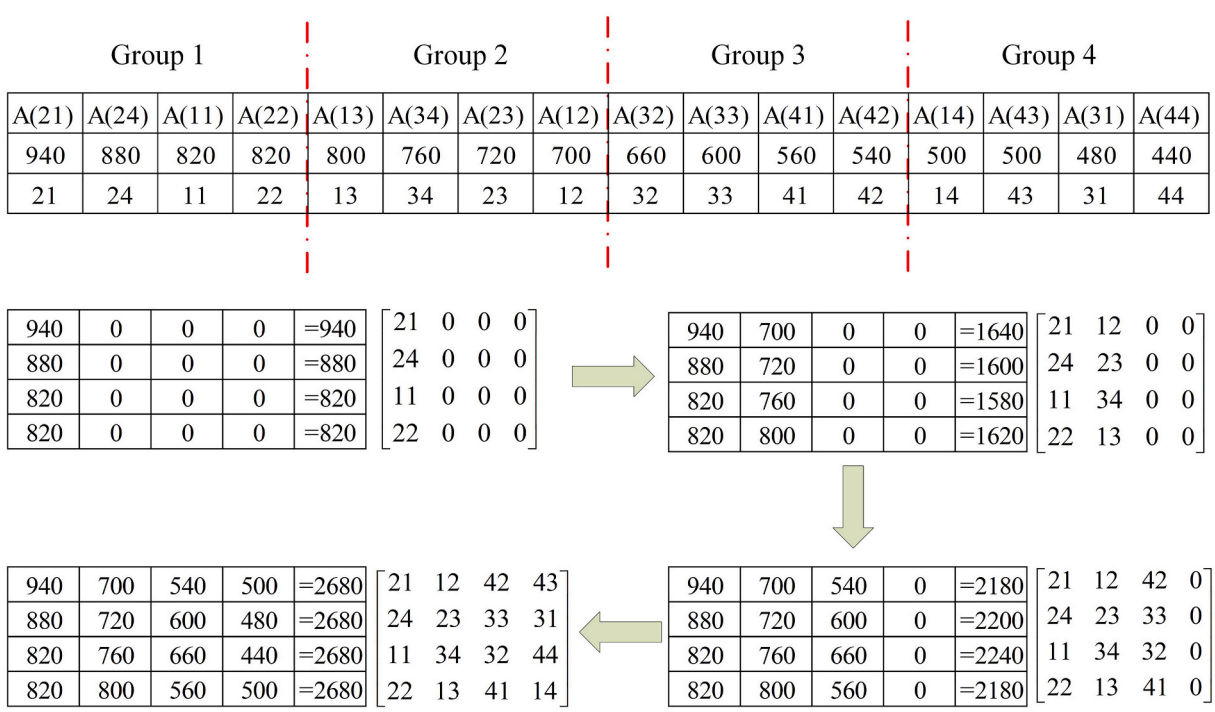

Fig. 8. Example of Smart Choice algorithm.

(c) If any adjustment is approved, update the C and C_{co} matrices, and repeat steps 1–5.

(d) If no adjustments are approved, this indicates that the current matrix C is the globally optimal matrix, and the algorithm terminates. The irradiance and coordinate matrices at this stage are D and D_{co}, respectively.

4.4. Munkres' assignment algorithm (MAA)

The MAA aims to optimize the coordinate matrix. The element M_{ij} in the cost matrix M is defined as the number of modules that exist in row i of the matrix A_{co} but not in row j of the intermediate matrix D_{co}. Taking the optimization process shown in Fig. 9, the algorithm proceeds as follows:

Step 1: Extract the initial coordinate matrix A_{co} (Fig. 9 (a)) and reconfigured intermediate coordinate matrix D_{co} (Fig. 9 (c)).

Step 2: Calculate the number of different elements between the i-th row of A_{co} and the j-th row of $D_{co}$and assign it to M_{ij}.

Step 3: Perform row transformations based on the minimum value in each row of the cost matrix M. Fig. 9 (b) shows that the coordinates of the minimum value in each row are (1,4), (2,2), (3,3), and (4,1), indicating that rows 1, 2, 3, and 4 are the closest to rows 4, 2, 3, and 1 of D_{co}, respectively. Therefore, swap rows 1 and 4 of the matrix D_{co} to obtain the final coordinate matrix E_{co}.

Step 4: Simultaneously transform the intermediate irradiation matrix D into the final irradiation matrix E.

4.5. Process of the multilevel optimization algorithm

The irradiance distribution of the PV array, which was calculated using the irradiance surface model described in Section 2.2, is shown in Fig. 10. The irradiance intensity of the PV modules varied between a maximum of 879 W/m^2 and a minimum of 435 W/m^2 depending on their position. The irradiance intensity varied smoothly along the axial and circumferential directions of the hull. By dividing the PV array into m × n modules, it is evident that the curvature of each module is significantly reduced, leading to a substantial decrease in irradiance variations. To facilitate the establishment of the irradiance matrix, in this study, the average irradiance value within each small region is considered as the equivalent irradiance intensity for the components.

The power output of the PV array varies with flight time, attitude, and geographic coordinates. Therefore, it is necessary to design a reconfiguration process that considers the flight states. In addition, a multilevel optimization strategy is employed. If the first optimization satisfies the performance requirements, the second optimization is omitted to further reduce the optimization time. The algorithm process is presented in Fig. 11 and is described as follows:

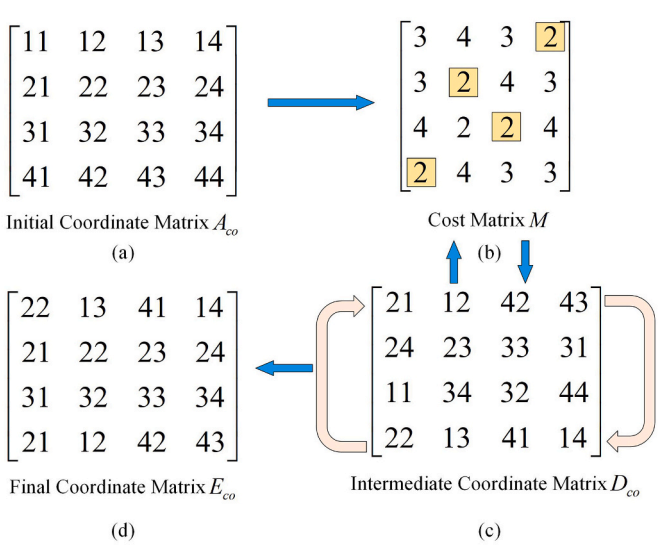

Fig. 9. Example of Munkres' assignment algorithm (MAA).

Step 1: Initiate the reconfiguration process every 5 min if the irradiance intensity obtained from the onboard irradiance intensity collection device is greater than 50 W/m^2.

Step 2: Retrieve the state information from the measurement and control equipment, which will be used as input for the equivalent irradiance calculation model to generate the initial irradiance matrix A and coordinate matrix A_{co}.

Step 3: Calculate the EI, I_{rowi}, and I_{rowavg} of matrix A, and determine the MPP of the PV array before reconfiguration.

Step 4: If $EI > I_{rowavg} \times 0.01$, it indicates that the current topology already satisfies the "irradiance equalization" criterion. In this case, return to step 2 and wait for updated parameters. Otherwise, proceed with the subsequent steps.

Step 5: Use the SC algorithm to reconfigure A and A_{co}, resulting in C and C_{co}, respectively. Calculate EI, I_{rowi}, and C. If $EI > I_{rowavg} \times 0.01$, proceed to step 6. Otherwise, skip step 6 and proceed to step 7.

Step 6: Use the GA to perform a second reconfiguration of C and C_{co}, resulting in matrices D and D_{co}, respectively.

Step 7: Perform a row transformation of matrices D and D_{co} using the MAA, resulting in matrices E and E_{co}.

Step 8: Calculate the MPP of the reconfigured PV arrayP_{mppre}. If P_{mppre} increases by more than 1%, generate the control vector based on the results of step 7, reconfigure the switch matrix, and update matrices A and A_{co}. Otherwise, skip the reconfiguration operation and return to step 1. Initiate the next reconfiguration process after a 5 min interval.

5. Results and discussion

5.1. Analysis of multi-operating condition examples

Table 1 presents the design parameters of the PV modules. Each pack comprised 48 modules connected in a 4 × 12 SP configuration, effectively forming a large PV pack. The PV array comprised 16 large PV packs connected in a 4 × 4 TCT configuration. Under uniform irradiation conditions (1000 W/m^2 @ 25℃), the array produced an open-circuit voltage of 712 V, short-circuit current of 404 A, and maximum power output of 204.8 kW.

Here, the winter solstice, which is characterized by the weakest irradiation in the Northern Hemisphere, was assumed as the simulated flight date. The operating conditions are listed in Table 2. Fig. 12 shows a comparison of the output characteristics and irradiance matrix of the PV array before and after reconfiguration under various operating conditions.

In ondition 1, the initial irradiance matrix had an EI of 628 W/m^2 (Fig. 12 (c)), whereas the reconfigured irradiance matrix had an EI of 9 W/m^2 (Fig. 12 (d)). The MPPs of the PV array before and after reconfiguration were 108.2 and 118 kW (Fig. 12 (a) and (b)), respectively, resulting in a 9.1% improvement. The reconfiguration process involved optimizing the irradiance matrix using only the SC algorithm; the GA was skipped, which enhanced the computational speed.

In condition 2, the pitch angle was raised to 8°, while the yaw angle was altered to 150°, causing an increase in the EI to 1041 W/m^2. Fig. 12 (e) shows the I—V curve with a step-down characteristic (black line), while Fig. 12 (f) displays the P—V curve (black line) with four local MPPs at 19.5, 31.5, 34.6, and 29.1 kW. This could potentially misguide the MPPT algorithm, and the MPP undergoes significant attenuation. Following the reconfiguration, the EI was reduced to 4 W/m^2 (Fig. 12 (h)), and the P—V curve displayed a single MPP characteristic (Fig. 12 (e), red line). The MPP increased to 52.2 kW, resulting in an improvement rate of 66.2%, which represented the maximum output capacity. By comparing the irradiance and coordinate matrices before and after reconfiguration (Fig. 12 (g) and (h)), it is evident that the global optimal solution was achieved by jointly optimizing the SC and GA algorithms.

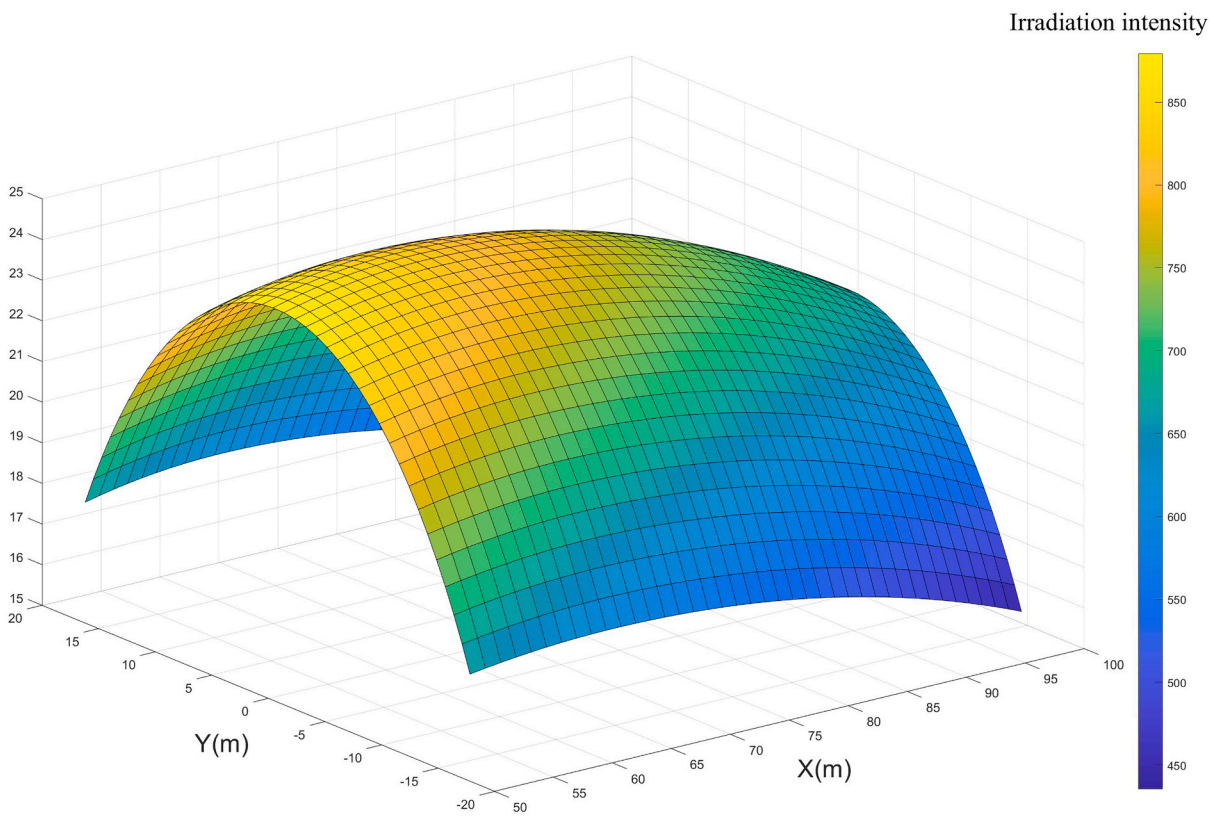

Fig. 10. Equivalent irradiance distribution of PV modules.

Condition 3 is analogous to condition 2. Before reconfiguration, the EI was 964 W/m^2 (Fig. 12 (k)), and the P—V curve exhibited four maximum power points with a maximum output power of 75.6 kW (Fig. 12 (j), black line). After joint optimization using the SC and GA algorithms, the EI was reduced to 36 W/m^2 (Fig. 12 (l)), and the maximum power increased to 94.2 kW (Fig. 12 (j), red line), resulting in a 24.6% improvement.

The optimization results showed that the PV array exhibited improvements before and after reconfiguration under different operating conditions. The SC algorithm was sufficient for obtaining the global optimal solution for operating conditions with small initial EI differences. However, joint optimization using both the SC and greedy algorithms is required to obtain the global minimum EI for operating conditions with significant EI differences. Pre-optimization using the SC algorithm can enhance computational speed by significantly reducing the number of exchanges and movements during the GA process.

5.2. Radiation period flight simulation

The optimal irradiance matrix for stratospheric airships varies owing to changes in the heading and pitch angles caused by the wind conditions and mission trajectories. Therefore, it is necessary to continuously reconstruct and optimize the irradiance matrix during periods of sun exposure, as detailed in Section 4.5.

A seven-day flight window was selected based on the weakest solar irradiance intensity, with the airship flying at an altitude of 20,000 m and located at 20°N and 105°E. Fig. 13 depicts the wind characteristics during this period, with red and blue lines representing the wind speed and direction, respectively. Wind speeds exceeding 60 km/h on Dec. 21 and 22 made the airship maneuvering unfavorable, and a fixed-position strategy was required. During this period, the airship maintained a headwind position to minimize energy consumption, with the heading angle matching the wind direction [51]. From Dec. 23 to 27, the average wind speed dropped to approximately 20 km/h, allowing cruise flights based on the mission requirements. Specifically, the airship cruised in a circular pattern with a 20 km radius, completing one circle every 2 h. Owing to wind disturbances and changes in the envelope pressure difference, the pitch angle fluctuated periodically, and Fig. 14 illustrates the changes in heading and pitch angles.

Fig. 15 and Fig. 16 compare the output power and daily output of the PV array before and after the reconfiguration, respectively. Table 3 summarizes the maximum power, Daily energy, and increase rate before and after reconfiguration. Irrespective of wind-resistant hovering (first two days) or maneuvering cruise (last five days), the output power and daily electricity generation exhibited an increase after the reconfiguration of the PV array compared to the pre-reconfiguration period. The highest improvement rate occurred on Dec. 23, with a daily energy generation increase of 141.4 kWh and an increase rate of 16.11%. On Dec. 22, the improvement rate was the lowest, with an increase of 128 kWh. Based on the 7-day simulation results, the average increase rate was approximately 14.68%, with a cumulative increase of 992.4 kWh in energy generation.

Dec. 21 and 25 were selected as representative operating conditions to assess the effects of the PV array reconfiguration on the system output status. Fig. 17 (a) and Fig. 17 (b) present a comparison of the PV array output power before and after reconfiguration during the 6:00–18:00 period on the selected days. On Dec. 21, the airship was in the wind-resistant flight mode, with the heading angle remaining stable between 250° and 275°. The power change trends before and after reconfiguration were consistent, with five significant power fluctuations caused by changes in pitch angle. Reconfiguration occurred during the two periods marked by the yellow dashed line in Fig. 17 (a), from 7:00–10:30 and 14:30–15:30, during which the airship's attitude angle changes had a significant impact on the PV array's irradiation distribution characteristics. During the process, a total of 19 reconfiguration operations were performed, with 4 times being optimized using the SC–MAA algorithm, while the remaining 15 times were optimized using the SC–GA–MAA algorithm.

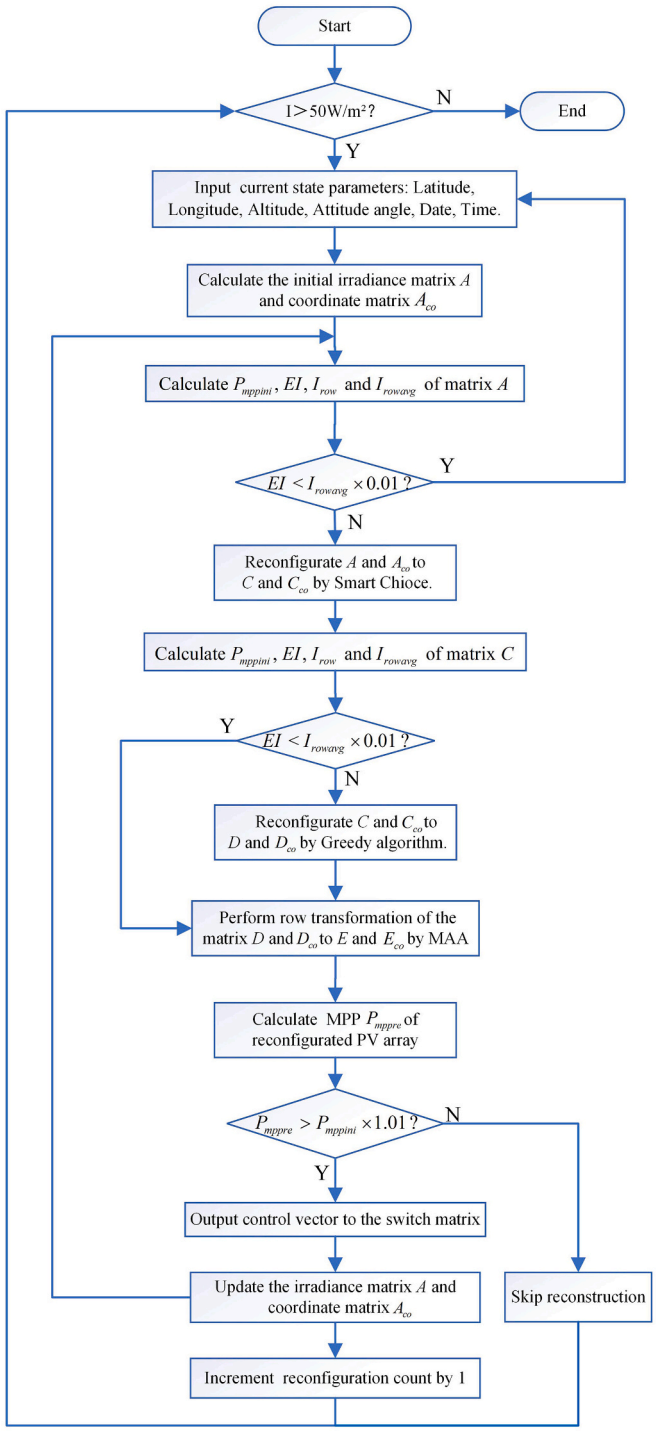

Fig. 11. Multilevel optimization algorithm flowchart.

On Dec. 25, the airship was in the circular cruising mode and completed 6 rounds of cruising during the sunshine period. The irradiation curve before reconfiguration is shown as a black line in Fig. 17 (b), with 6 significant power fluctuations in line with the periodic changes in the yaw angle. 33 reconfiguration operations were performed, with 5 and 27 times using the SC–MAA and SC–GA–MAA algorithms, respectively. The SC-MAA algorithm is typically employed during noon when the irradiation distribution is relatively uniform. However, in most cases, achieving the optimal configuration necessitates a combined optimization using the SC-GA-MAA algorithms. During the two reconfiguration periods, 7:00–10:00 and 15:00–17:30, the PV array output power change was smoother (red line in Fig. 17 (b)), and the power increase was most significant at the original concave points. Moreover, during the periods without reconfiguration, the output power fluctuation was smaller. The reconfiguration improved the output power and stability of the PV array, reducing the impact of periodic changes in the yaw angle on the PV system under such operating conditions.

Table 1
Design parameters for PV module.

Parameter	Value
Maximum power	267 W
Open circuit voltage	44.5 V
Short circuit current	8.42 A
Maximum power point voltage	35.1 V
Maximum power point current	7.69 A
Series number of PV modules	4
Parallel number of PV modules	12
Series number of PV array	4
Parallel number of PV array	4

5.3. Energy increase rate of reconfiguration

The net energy output increase and energy increase rate of the PV array due to the reconfigured system was statistically analyzed for latitudes between 18° and 48° throughout the year. The simulation conditions were consistent, with the airship completing a circular cruise every 2 h and the pitch angle cyclically varying between −10° and + 10°.

Fig. 18 (a) shows the contribution of the reconfigured system at different latitudes to the net energy enhancement of the PV system throughout the year. In the mid-to low-latitude regions of 18° to 25°, where the solar altitude angle changes relatively little throughout the year, the irradiation conditions were stable, and the improvement in the PV array output energy owing to reconfiguration was close, ranging from 138.8 to 153.2 kWh. However, the output enhancement rate was subject to certain fluctuations owing to the influence of the pitch angle. As the latitude increased, the net energy enhancement gradually increased from 145 kWh (18°N) to 165.3 kWh (48°N) from May to September. Conversely, the net energy enhancement exhibited a significant decreasing trend in November, December, and January, dropping from 149 to 81 kWh. This is because daylight hours are longer in summer in high-latitude regions, resulting in a higher daily output for the PV system and an increase in net energy enhancement. In contrast, during weaker irradiation conditions in winter, the PV system output capacity gradually decreased with an increase in the altitude angle, leading to a reduction in the net energy increase.

As shown in Fig. 18 (b), the energy increase rate trend is opposite to that of the net energy enhancement. From April to August, the increase rates in both the low- and high-latitude regions were similar, ranging from 9.6% to 11.2%. In the remaining months, the increase rate significantly increased with latitude, reaching 24.46% near the winter solstice at 48°N. In the same latitude region, the energy increase rate of the PV array in different months exhibited an opposite trend to that of the total daily output energy. This is because in autumn and winter, when the solar altitude angle is low, the PV mismatch loss caused by the airship attitude angle variation is more severe. The gain from reducing the mismatch loss through the PV reconfiguration system is greater. This indicates that the reconfigured system is more advantageous in months with weaker irradiance, and that the higher the latitude, the more significant the increase in the PV system output.

From the perspective of the stratospheric airship design, the energy system must satisfy the energy-balance requirements of the flight envelope with the weakest irradiation. According to the analysis shown in Fig. 18 (b), the advantage of the PV reconfiguration system increases as the irradiation weakens. Therefore, the reconfigured system can significantly reduce the weight and installation area of the PV array carried by

Table 2
Simulation conditions.

Condition	Date	Coordinate	Time	Pitch angle	Yaw angle	MPP before reconfigure	MPP after reconfigure	Increase rate
1	12.23	18°N	10:00	0°	0°	108.2 kW	118.9 kW	9.8%
2		105°E	9:30	8°	150°	34.6 kW	51.9 kW	50.1%
3			15:00	-5°	250°	75.6 kW	93 kW	23%

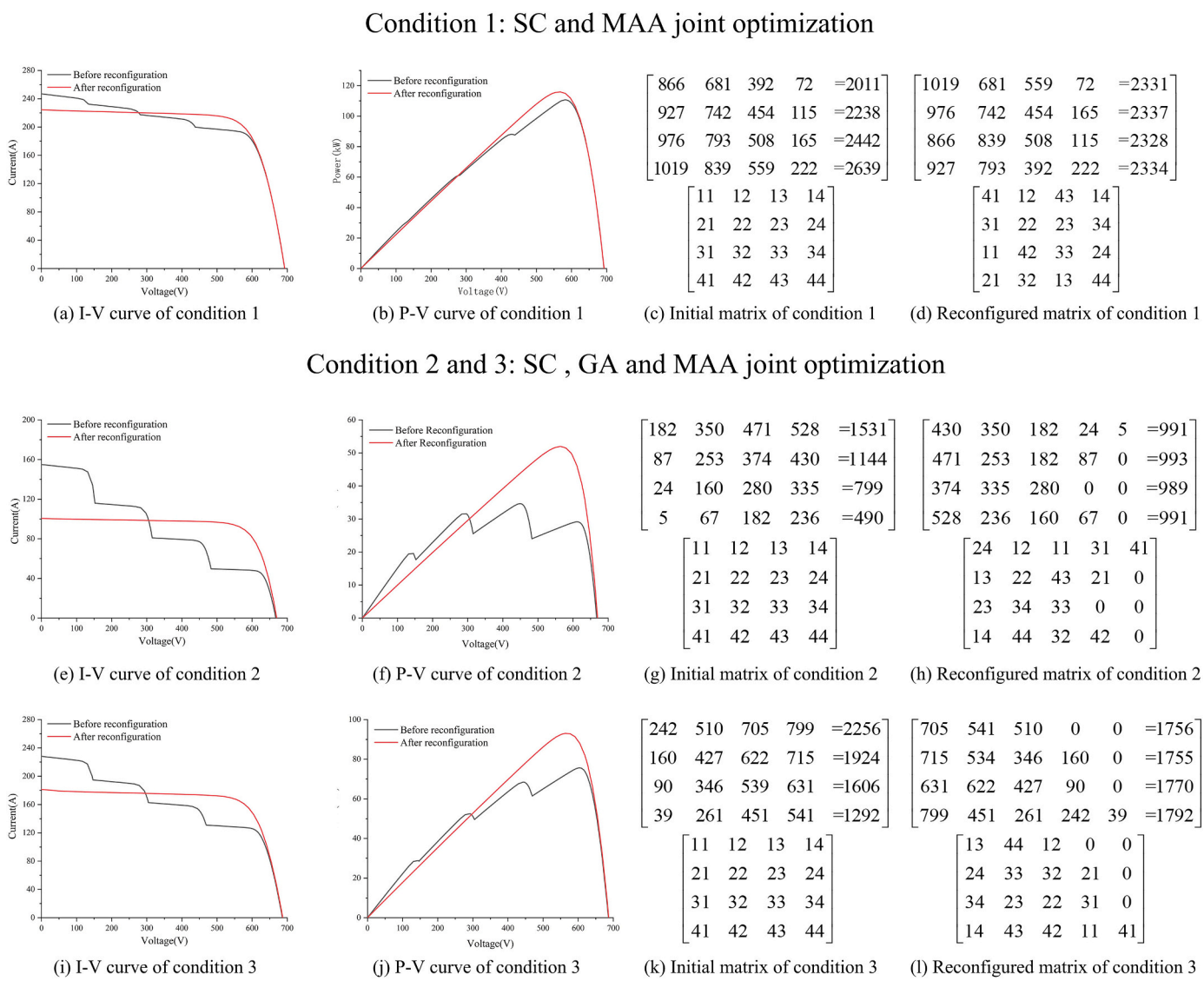

(a) I-V curve of condition 1 (b) P-V curve of condition 1 (c) Initial matrix of condition 1 (d) Reconfigured matrix of condition 1

(e) I-V curve of condition 2 (f) P-V curve of condition 2 (g) Initial matrix of condition 2 (h) Reconfigured matrix of condition 2

(i) I-V curve of condition 3 (j) P-V curve of condition 3 (k) Initial matrix of condition 3 (l) Reconfigured matrix of condition 3

Fig. 12. Comparison of PV array Characteristics before and after reconfiguration.

the airship.

6. Conclusion

This study analyzed the reasons for the mismatch losses of PV arrays carried by stratospheric airships. A PV array reconfiguration system that can effectively reduce the mismatch losses of the PV array carried by stratospheric airships and improve the output power is proposed. A multilevel reconfiguration optimization algorithm was designed. Finally, a simulation verification was conducted to compare the output characteristics before and after the reconfiguration, and to analyze the changes in the system improvement rate under different operating conditions. The conclusions are as follows:

(1) Changes in yaw and pitch angles are the main causes of PV system mismatch. The PV mismatch causes the actual output power of the array to be much lower than the theoretical output power, and the P—V curve of the array may contain multiple MPPs, which can mislead the MPPT algorithm and further reduce the output power.

(2) The multilevel reconfiguration optimization algorithm can adapt to the irradiation matrix characteristics under different operating conditions while ensuring that the solution result is the global optimum and increases the solution speed. The output power of the reconfigured PV array was improved by varying degrees, and under extreme operating conditions, the instantaneous output power was increased by 50.1%. In addition, the multiple MPP

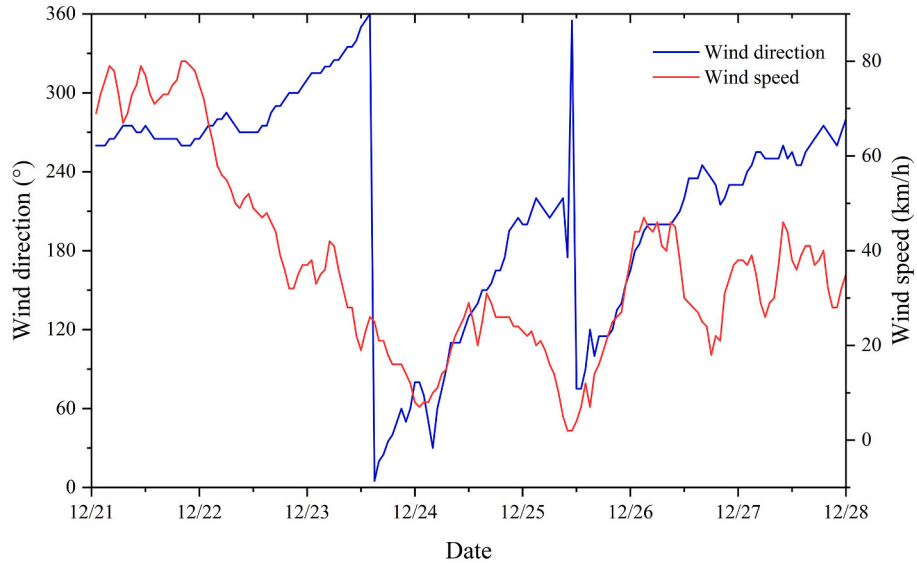

Fig. 13. Wind speed and direction from December 21 to 27.

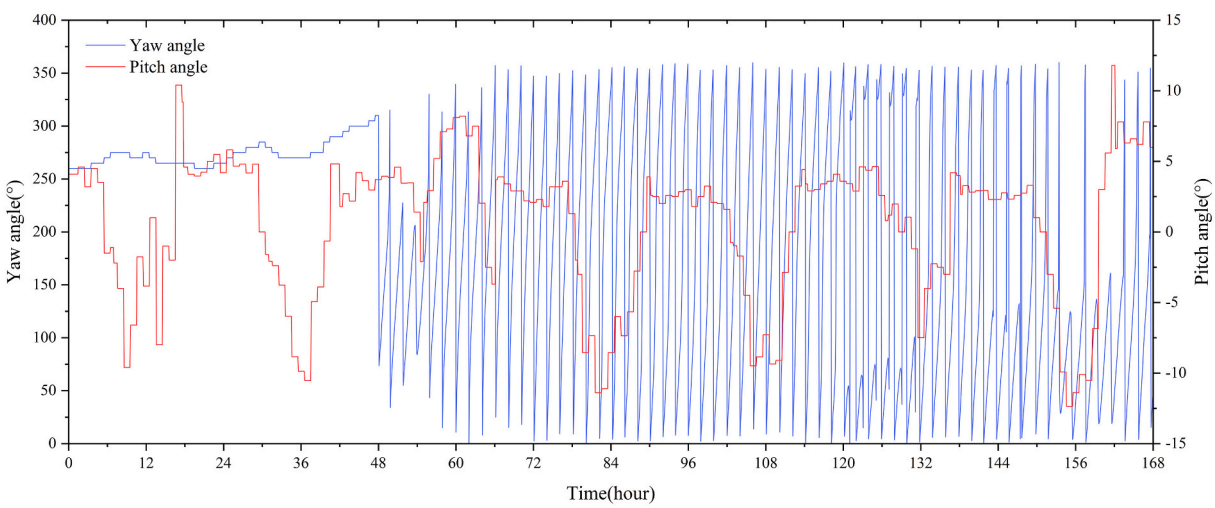

Fig. 14. Attitude angles of the airship from December 21 to 27.

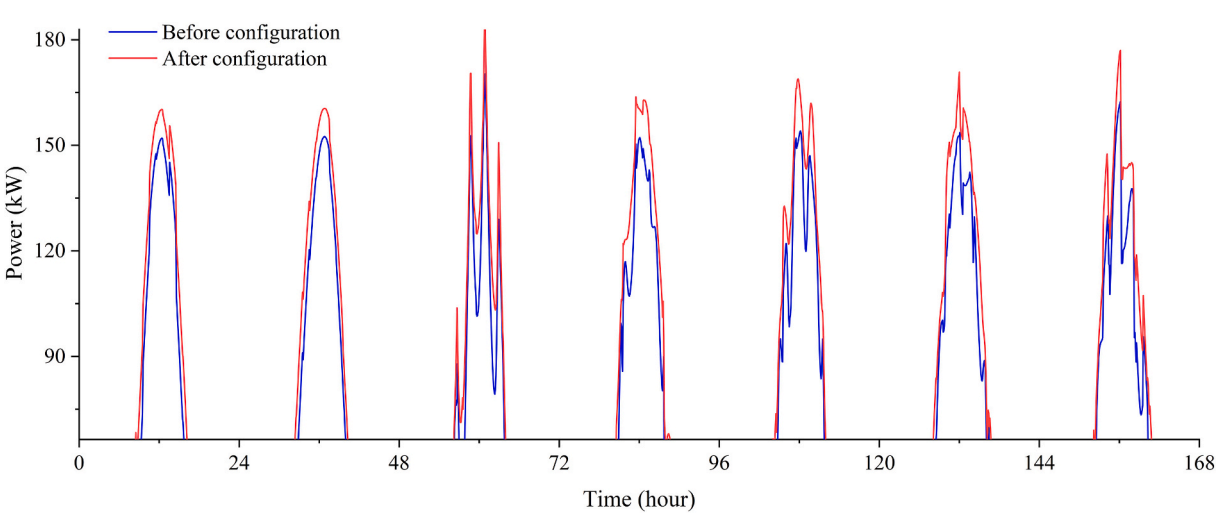

Fig. 15. Comparison of PV array output power.

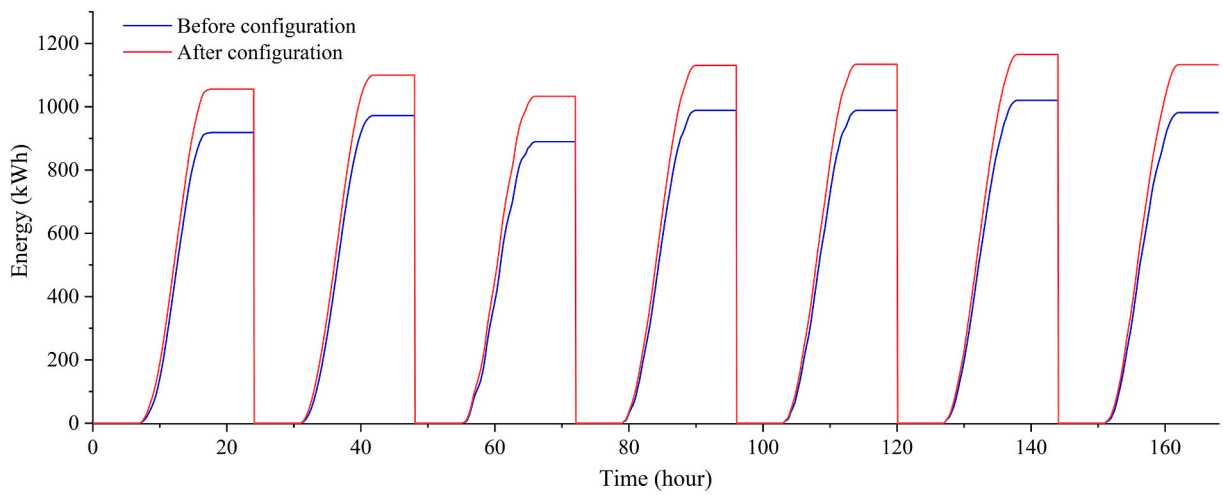

Fig. 16. Comparison of PV array output energy.

Table 3
Power and energy calculation for reconfiguration.

Date	Before reconfiguration		After reconfiguration		Maximum Power increase rate (%)	Daily power generation increase rate (%)
	Maximum output power (kW)	Daily power generation (kWh)	Maximum output power (kW)	Daily power generation (kWh)		
Dec. 21	151.9	918.5	160	1055.7	5.33	14.94
Dec. 22	152.5	967.2	160.4	1100.2	5.18	13.75
Dec. 23	170.2	889.5	187.5	1032.8	10.16	16.11
Dec. 24	152.1	988.6	163.7	1130.7	7.63	14.37
Dec. 25	153.6	988.7	168.8	1134.2	9.89	14.72
Dec. 26	153.4	1020.4	170.7	1165.2	11.28	14.19
Dec. 27	162.4	981.5	176.9	1133.5	8.93	15.49

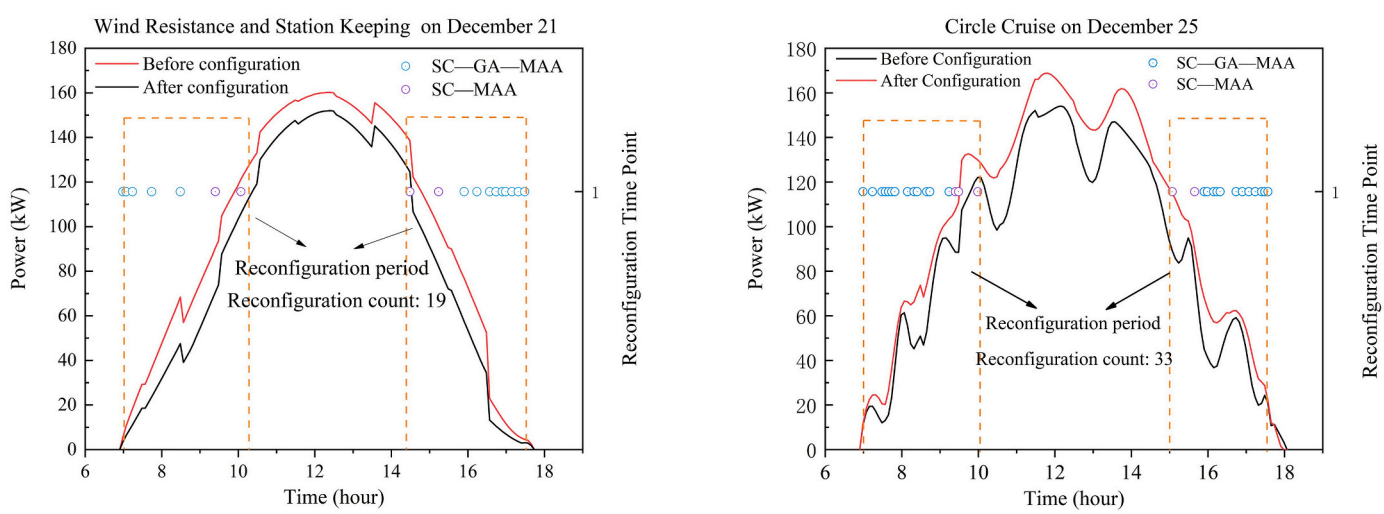

（a）Wind resistance and station keeping on December 21 （b）Circle Cruise on December 25

Fig. 17. Comparison of output power on December 21 and 25.

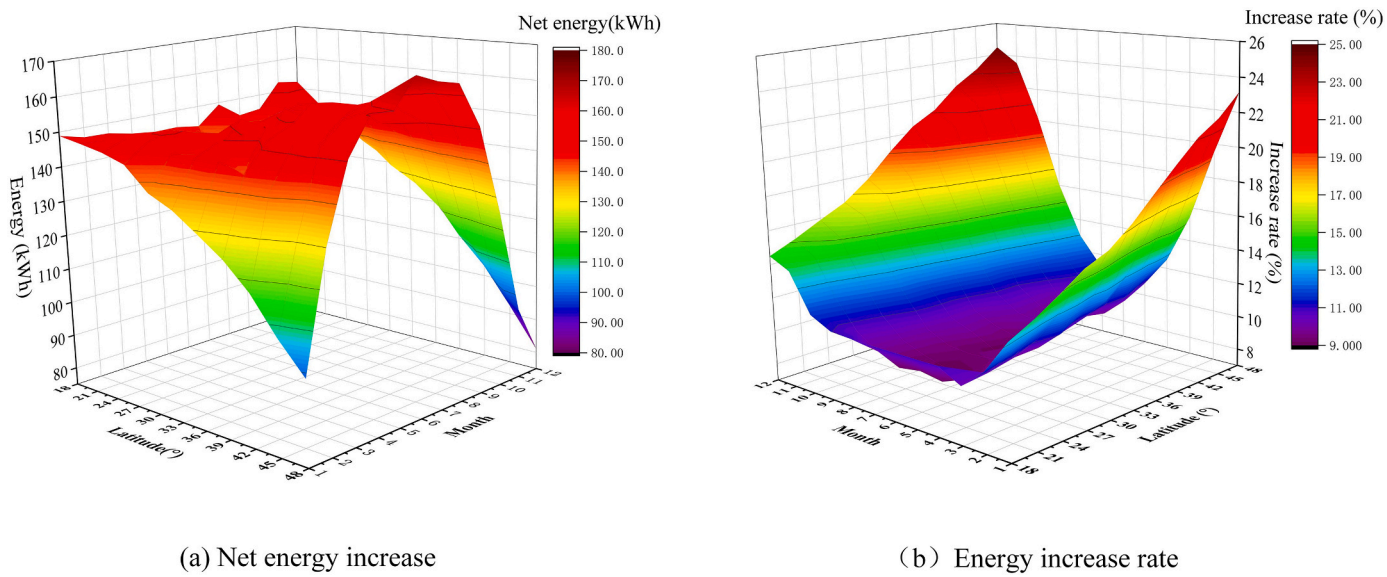

(a) Net energy increase

(b) Energy increase rate

Fig. 18. Statistics of PV reconfiguration system energy increase.

points of the P—V curve were optimized to a single MPP point, eliminating misleading effects on the MPPT algorithm.

(3) The reconfiguration can improve the PV array output power and supply stability for circular cruising with periodic changes in the yaw angle. During the 7-day simulation flight, the reconfigured PV array increased the total output energy by approximately 14.68%, thereby increasing the cumulative power generation 997.9 kWh.

(4) The PV reconfiguration system has greater advantages in weakly irradiated months. The higher the latitude is, the more obvious the improvement in the energy output of the PV system, with an increased rate of up to 24.46% on the winter solstice at 48°N. Introducing the reconfiguration system in the energy system design, simulation, and optimization phases can provide more accurate output characteristics and significantly reduce the installation area and weight of the PV array.

CRediT authorship contribution statement

Chuan Shan: Writing – original draft, Software, Methodology, Conceptualization. **Kangwen Sun:** Visualization, Investigation, Data curation. **Xinzhe Ji:** Writing – review & editing, Validation, Formal analysis. **Dongji Cheng:** Supervision, Investigation.

Declaration of Competing Interest

The authors declare that they have no known competing financial interests or personal relationships that could have appeared to influence the work reported in this paper.

Data availability

No data was used for the research described in the paper.

Acknowledgements

This work was supported by the National Natural Science Foundation of China [grant numbers 51775021], the Fundamental Research Funds for the Central Universities [grant numbers YWF-23-JC-01, YWF-23-JC-02, YWF-23-JC-03, YWF-23-JC-04, YWF-23-JC-09].

References

[1] Gou HB, Zhu M, Zheng ZW, Guo X, Lou WJ, et al. Adaptive fault-tolerant control for stratospheric airships with full-state constraints, input saturation, and external disturbances [J]. Adv Space Res 2022;69(1):701–17. https://doi.org/10.1016/j.asr.2021.09.015.

[2] Arum SC, Grace D, Mitchell PD. A review of wireless communication using high-altitude platforms for extended coverage and capacity [J]. Comput Commun 2020;157:232–56. https://doi.org/10.1016/j.comcom.2020.04.020.

[3] Manikandan M, Pant RS. Research and advancements in hybrid airships—a review [J]. Progr Aerosp Sci 2021;3:100741. https://doi.org/10.1016/j.paerosci.2021.100741.

[4] Zhang L, Li J, Wu Y, Lv M. Analysis of attitude planning and energy balance of stratospheric airship [J]. Energy 2019;183:1089–103. https://doi.org/10.1016/j.energy.2019.07.002.

[5] Gao WN, Zhang J, Ma T, Lin GC, Liu YP, et al. A novel inflatable rings supported design and buoyancy-weight balance deformation analysis of stratosphere airships [J]. Chin J Aeronaut 2022;35(1):340–7. https://doi.org/10.1016/j.cja.2020.11.019.

[6] Shen L, Li ZP, Ma T. Analysis of the power loss and quantification of the energy distribution in PV module [J]. Appl Energy 2020;260:114333. https://doi.org/10.1016/j.apenergy.2019.114333.

[7] Yue QL, He CX, Wu MC, et al. Advances in thermal management systems for next-generation power batteries [J]. Int J Heat Mass Transf 2021;181:121853. https://doi.org/10.1016/j.ijheatmasstransfer.2021.121853.

[8] Liao J, Jiang Y, Li J, et al. An improved energy management strategy of hybrid photovoltaic/battery/fuel cell system for stratospheric airship [J]. Acta Astronaut 2018;152:727–39. https://doi.org/10.1016/j.actaastro.2018.09.007.

[9] Zhang J, Xuan Y, Yang L. A novel choice for the photovoltaic–thermoelectric hybrid system: the perovskite solar cell [J]. Int J Energy Res 2016;40(10):1400–9. https://doi.org/10.1002/er.3532.

[10] Yunce Zhang, Yafei Wang, Changguo Wang. Light weight optimization of stratospheric airship envelope based on reliability analysis [J]. Chin J Aeronaut 2020;33(10):2670–8. https://doi.org/10.1016/j.cja.2020.04.012.

[11] Wang HF, Song BF, Zuo LK. Effect of high-altitude airship's attitude on performance of its energy system [J]. J Aircr 2007;44(6):2077–80. https://doi.org/10.2514/1.31505.

[12] Lv MY, Li J, Du HF, Zhu WY, Meng JH. Solar array layout optimization for stratospheric airships using numerical method [J]. Energ Conver Manage 2017;135:160–9. https://doi.org/10.1016/j.enconman.2016.12.080.

[13] Li J, Lv MY, Tan DJ, Zhu WY, Sun KW. Output performance analyses of solar array on stratospheric airship with thermal effect [J]. Appl Therm Eng 2016;104:743–50. https://doi.org/10.1016/j.applthermaleng.2016.05.122.

[14] Alam MI, Pant RS. Multi-objective multidisciplinary design analyses and optimization of high altitude airships [J]. Aerosp Sci Technol 2018;78:248–59. https://doi.org/10.1016/j.ast.2018.04.028.

[15] Zhu WY, Li J, Xu YM. Optimum attitude planning of near-space solar powered airship [J]. Aerosp Sci Technol 2019;84:291–305. https://doi.org/10.1016/j.ast.2018.10.007.

[16] Shan C, Lv MY, Sun KW, Jian G. Analysis of energy system configuration and energy balance for stratospheric airship based on position energy storage strategy [J]. Aerosp Sci Technol 2020;101:105844. https://doi.org/10.1016/j.ast.2020.105844.

[17] Gao Y, Dong JF, Isabella O, Santbergen R, Tan HR, et al. Modeling and analyses of energy performances of photovoltaic greenhouses with sun-tracking functionality

[J]. Appl Energy 2019;233:424–42. https://doi.org/10.1016/j.apenergy.2018.10.019.
[18] Lv MY, Li J, Zhu WY, Du HF, Meng JH, et al. A theoretical study of rotatable renewable energy system for stratospheric airship [J]. Energ Conver Manage 2017;140:51–61. https://doi.org/10.1016/j.enconman.2017.02.069.
[19] Du HF, Li J, Zhu WY, Yao ZB, Cui EQ, et al. Thermal performance analysis and comparison of stratospheric airships with rotatable and fixed photovoltaic array [J]. Energ Conver Manage 2018;158:373–86. https://doi.org/10.1016/j.enconman.2017.12.078.
[20] Zhu WY, Xu YM, Li J, Zhang LC. Performance analysis of rotatable energy system of high-altitude airships in real wind field [J]. Aerosp Sci Technol 2020;98:105689. https://doi.org/10.1016/j.ast.2020.105689.
[21] Liu Y, Sun KW, Xu ZY, Lv MY. Energy efficiency assessment of photovoltaic array on the stratospheric airship under partial shading conditions [J]. Appl Energy 2022;325:119898. https://doi.org/10.1016/j.apenergy.2022.119898.
[22] Velasco-Quesada G, Guinjoan-Gispert F, Pique-Lopez R, et al. Electrical PV Array reconfiguration strategy for energy extraction improvement in grid-connected PV systems [J]. IEEE Trans Indust Electr 2009;56(11):4319–31. https://doi.org/10.1109/TIE.2009.2024664.
[23] Roberto Candela, Riva Sanseverino Eleonora, Pietro Romano, et al. A Dynamic Electrical Scheme for the optimal reconfiguration of PV modules under non-homogeneous solar irradiation. In: Proceedings of the International Conference on Mechanical Science and Engineering. F; 2012.
[24] Romano P, Candela RC. Optimization of photovoltaic energy production through an efficient switching matrix [J]. J Sustain Dev Energy Water Environ Syst 2013;1(3):227–36. https://doi.org/10.13044/j.sdewes.2013.01.0017.
[25] Sanseverino ER, Ngoc TN, Cardinale M, Li Vigni V, Musso D, et al. Dynamic programming and Munkres algorithm for optimal photovoltaic arrays reconfiguration [J]. Solar Energy 2015;122:347–58. https://doi.org/10.1016/j.solener.2015.09.016.
[26] Jazayeri M, Jazayeri K, Uysal S. Adaptive photovoltaic array reconfiguration based on real cloud patterns to mitigate effects of non-uniform spatial irradiance profiles [J]. Solar Energy 2017;155:506–16. https://doi.org/10.1016/j.solener.2017.06.052.
[27] Parlak KS. PV array reconfiguration method under partial shading conditions [J]. Int J Electr Power Energy Syst 2014;63:713–21. https://doi.org/10.1016/j.ijepes.2014.06.042.
[28] Karakose M, Baygin M, Parlak KS, et al. A new real-time reconfiguration approach based on neural network in partial shading for PV arrays. In: Proceedings of the 3rd International Conference on Renewable Energy Research and Application (ICRERA), Milwaukee, WI, F Oct 19–22, 2014 [C]; 2014.
[29] Karakose M, Baygin M, Murat K, et al. Fuzzy based reconfiguration method using intelligent partial shadow detection in PV arrays [J]. Int J Comput Intell Syst 2016;9(2):202–12. https://doi.org/10.1080/18756891.2016.1150004.
[30] Babu TS, Ram JP, Dragicevic T, et al. Particle swarm optimization based solar PV Array reconfiguration of the maximum power extraction under partial shading conditions [J]. IEEE Trans Sustain Energy 2018;9(1):74–85. https://doi.org/10.1109/TSTE.2017.2714905.
[31] Yousri D, Thanikanti SB, Balasubramanian K, et al. Multi-objective grey wolf optimizer for optimal design of switching matrix for shaded PV array dynamic reconfiguration [J]. IEEE Access 2020;8:159931–46. https://doi.org/10.1109/ACCESS.2020.3018722.
[32] Ahmed Fathy. Recent meta-heuristic grasshopper optimization algorithm for optimal reconfiguration of partially shaded PV array [J]. Solar Energy 2018;171:638–51. https://doi.org/10.1016/j.solener.2018.07.014.
[33] Nguyen D, Lehman B. An adaptive solar photovoltaic array using model-based reconfiguration algorithm [J]. IEEE Trans Indust Electr 2008;55(7):2644–54. https://doi.org/10.1109/TIE.2008.924169.
[34] Chao KH, Lai PL, Liao BJ. The optimal configuration of photovoltaic module arrays based on adaptive switching controls [J]. Energ Conver Manage 2015;100:57–67. https://doi.org/10.1016/j.enconman.2015.04.080.
[35] Cynthiachristabel S, Srinivasan A, Prince Winston D. Couple matching best generation algorithm for partially shaded photovoltaic systems [J]. J Electr Eng 2016;16:382–91.
[36] Ramasamy S, Seenithangam J, Dash SS, et al. A dodging algorithm to reconfigure photovoltaic array to negate partial shading effect [J]. Progr Photovolt 2016;24(2):200–10. https://doi.org/10.1002/pip.2661.
[37] Yang XX, Liu DN. Renewable power system simulation and endurance analysis for stratospheric airships [J]. Renew Energy 2017;113:1070–6. https://doi.org/10.1016/j.renene.2017.06.077.
[38] Hongjun Ran, Reid Thomas, Dimitri Mavris. A comprehensive global model of broadband direct solar radiation for solar cell simulation [M]. In: 45th AIAA Aerospace Sciences Meeting and Exhibit; 2023.
[39] Lv MY, Li J, Zhu WY, Du HF, Meng JH, et al. A theoretical study of rotatable renewable energy system for stratospheric airship [J]. Energ Conver Manage 2017;140:51–61. https://doi.org/10.1016/j.enconman.2017.02.069.
[40] Li J, Lv MY, Tan DJ, Zhu WY, Sun KW, et al. Output performance analyses of solar array on stratospheric airship with thermal effect [J]. Appl Therm Eng 2016;104:743–50. https://doi.org/10.1016/j.applthermaleng.2016.05.122.
[41] Du HF, Lv MY, Jun Li, Zhu WY, Zhang LC. Station-keeping performance analysis for high altitude balloon with altitude control system [J]. Aerosp Sci Technol 2019;92:644–52. https://doi.org/10.1016/j.ast.2019.06.035.
[42] Li J, Liao J, Liao YX, et al. An approach for estimating perpetual endurance of the stratospheric solar-powered platform [J]. Aerosp Sci Technol 2018;79:118–30. https://doi.org/10.1016/j.ast.2018.05.035.
[43] Wang YJ, Hsu PC. An investigation on partial shading of PV modules with different connection configurations of PV cells [J]. Energy 2011;36(5):3069–78. https://doi.org/10.1016/j.energy.2011.02.052.
[44] Akram MW, Li GQ, Jin Y, Chen X. Failures of photovoltaic modules and their detection: a review [J]. Appl Energy 2022;313:118822. https://doi.org/10.1016/j.apenergy.2022.118822.
[45] La Manna D, Vigni VL, Sanseverino ER, Di Dio V. Reconfigurable electrical interconnection strategies for photovoltaic arrays: a review [J]. Renew Sustain Energy Rev 2014;33:412–26. https://doi.org/10.1016/j.rser.2014.01.070.
[46] Belhachat F, Larbes C. PV array reconfiguration techniques for maximum power optimization under partial shading conditions: a review [J]. Solar Energy 2021;230:558–82. https://doi.org/10.1016/j.solener.2021.09.089.
[47] Balato M, Costanzo L, Vitelli M. Series-parallel PV array re-configuration: maximization of the extraction of energy and much more [J]. Appl Energy 2015;159:145–60. https://doi.org/10.1016/j.apenergy.2015.08.073.
[48] Chao KH, Lin YS, Lai UD. Improved particle swarm optimization for maximum power point tracking in photovoltaic module arrays [J]. Appl Energy 2015;158:609–18. https://doi.org/10.1016/j.apenergy.2015.08.047.
[49] Ngo TN, Phung QN, Tung LN, Sanseverino ER, Romano P, et al. Increasing efficiency of photovoltaic systems under non-homogeneous solar irradiation using improved dynamic programming methods [J]. Solar Energy 2017;150:325–34. https://doi.org/10.1016/j.solener.2017.04.057.
[50] Mahmoud Y, El-Saadany EF. Enhanced reconfiguration method for reducing mismatch losses in PV systems [J]. IEEE J Photovolt 2017;7(6):1746–54. https://doi.org/10.1109/JPHOTOV.2017.2752708.
[51] Jiang Y, Lv MY, Sun KW. Effects of installation angle on the energy performance for photovoltaic cells during airship cruise flight [J]. Energy 2022;258:124982. https://doi.org/10.1016/j.energy.2022.124982.